BASICS OF MOLECULAR BEAM-SURFACE SCATTERING

Vanessa J. Murray and Timothy K. Minton
Department of Chemistry and Biochemistry
Montana State University
Bozeman, MT 59715
tminton@montana.edu

Experiments analyzing the kinetics of gas-surface processes, such as carbon oxidation, provide information on the overall reaction rate of CO and CO_2 formation and mass loss.[1-3] However, these experiments do not reveal *how* the surface reactions proceed. Molecular beam-surface scattering experiments can determine the atomic level details of gas-surface interactions.[4] The flux and energy distributions of the scattered atoms and molecules can also provide qualitative information about the potential energy surface which governs the fate of a molecule that collides with the surface. By studying the outcome of gas-surface interactions, we can develop an atomistic understanding of the mechanisms by which reactive and nonreactive processes proceed.

In molecular beam-surface scattering experiments, the number density of the scattered products is measured as a function of flight time, $N(t)$. These plots are commonly referred to as time-of-flight (TOF) distributions, an example of which is shown in Figure 2.1. The TOF distributions are collected for specific final angles, θ_f, corresponding to an incidence angle, θ_i. A schematic of the experimental set up is shown in Figure 2.2. The flux of the scattered products is determined from the TOF distributions by integrating $N(t)/t$. A plot of the scattered flux as a function of θ_f is referred to as an angular distribution. The average energy of the scattered products is determined from translational energy distributions, $P(E_T)$, which are proportional to flux and derived from the TOF distributions by using a coordinate transformation and density-to-flux conversion[5, 6]

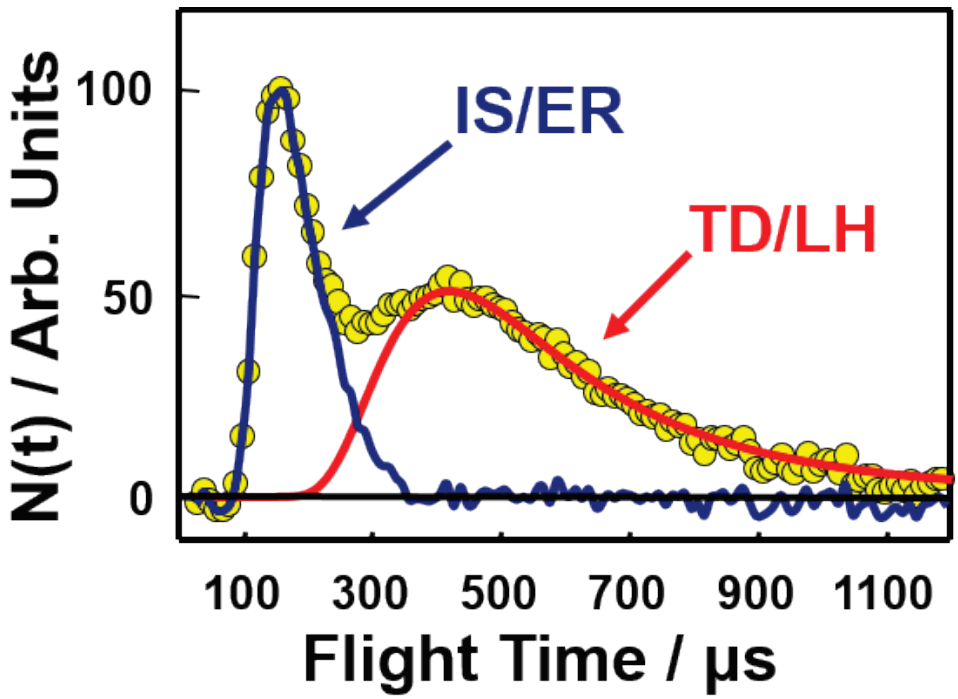

Figure 2.1. Example time-of-fight (TOF) distribution. The yellow symbols represent the total signal, *N(t)*. The blue line represents the impulsive scattering (IS) or Eley-Rideal (ER) signal. The red line represents the thermal desorption (TD) or Langmuir-Hinshelwood (LH) signal.

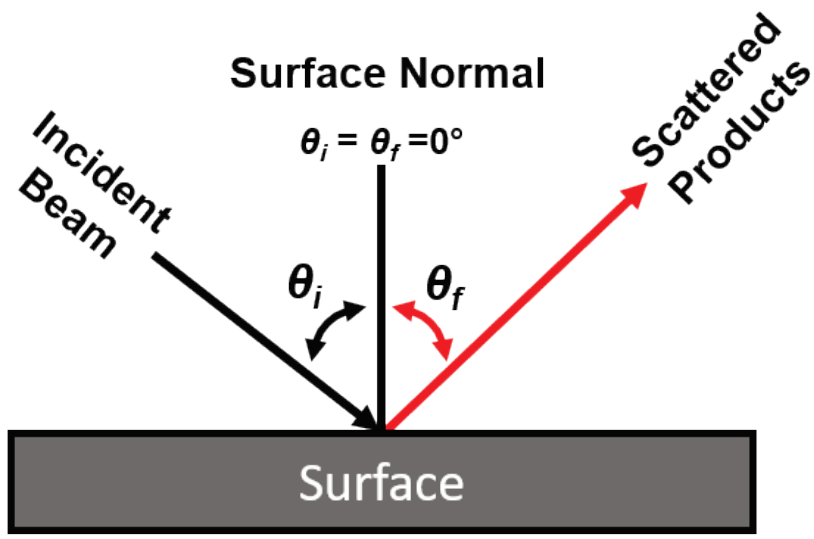

Figure 2.2. Simplified schematic of the molecular beam-surface scattering experiments showing the orientation of the incidence angle, θ_i, of the molecular beam and the final angle, θ_f, of the scattered products.

$$P(E_T) \propto t^2 N(t) \tag{2.1}$$

The translational energy, E_T, is given by

$$E_T = \frac{1}{2} m \left(\frac{d}{t}\right)^2 \tag{2.2}$$

where m is the mass of the detected product and d is the distance from the surface to the detector. By scrutinizing the shapes of the TOF distributions, angular distributions, and the $P(E_T)$ distributions, the dynamics of the scattered products can be determined. The remainder of this document will give a brief introduction to the unique experimental features of some gas-surface scattering mechanisms.

2.1 Nonreactive Scattering

2.1A Impulsive scattering

Atoms and molecules that scatter from the surface after one or a few collisions without reacting are said to undergo impulsive scattering (IS). The molecules have sufficient incidence energy, E_i, that they scatter from the repulsive wall of the potential energy surface without becoming trapped in the potential well (Figure 2.3, blue curve). The IS products retain most of their E_i and appear at short flight times in the TOF distribution (Figure 2.1, blue line).

The angular dependence of the final energy, E_f, for molecules that scatter via the IS channel can be divided into the thermal and structural scattering regimes.[7] When the E_i of the incident molecule is low, the turning point of the collision for the molecule is far from the surface and the molecule experiences a smooth potential energy surface (Figure 2.4,

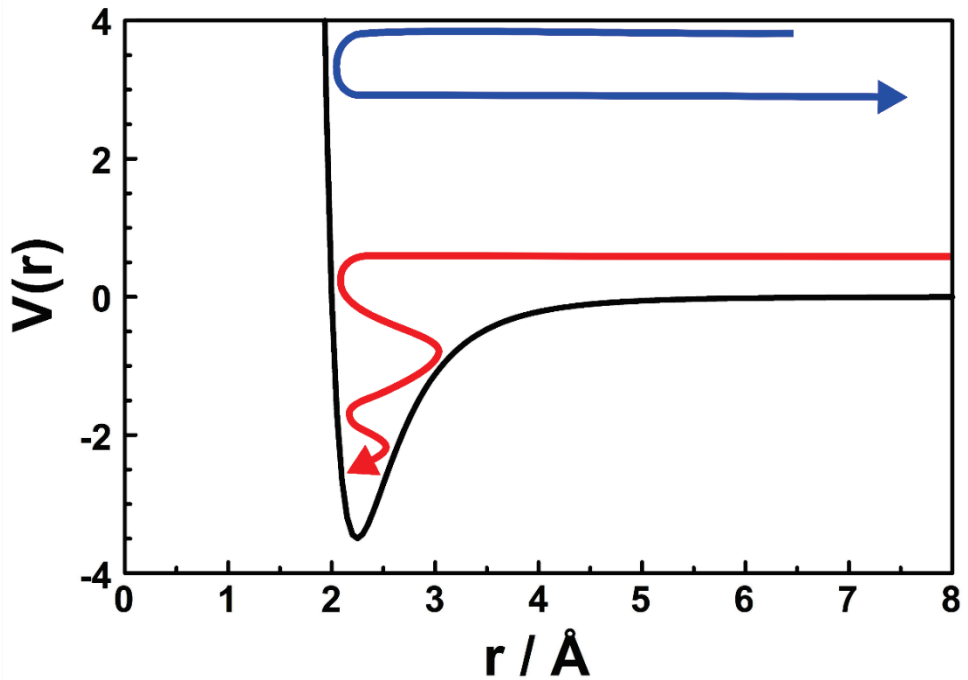

Figure 2.3. Schematic representation of a one-dimensional potential energy surface with no barrier to adsorption; r is the distance between the molecule and the surface. The position of the surface is defined as r = 0 Å. The blue line represents molecules that scatter via an IS mechanism. The red line represents molecules that stick to the surface before exiting the surface via a TD mechanism.

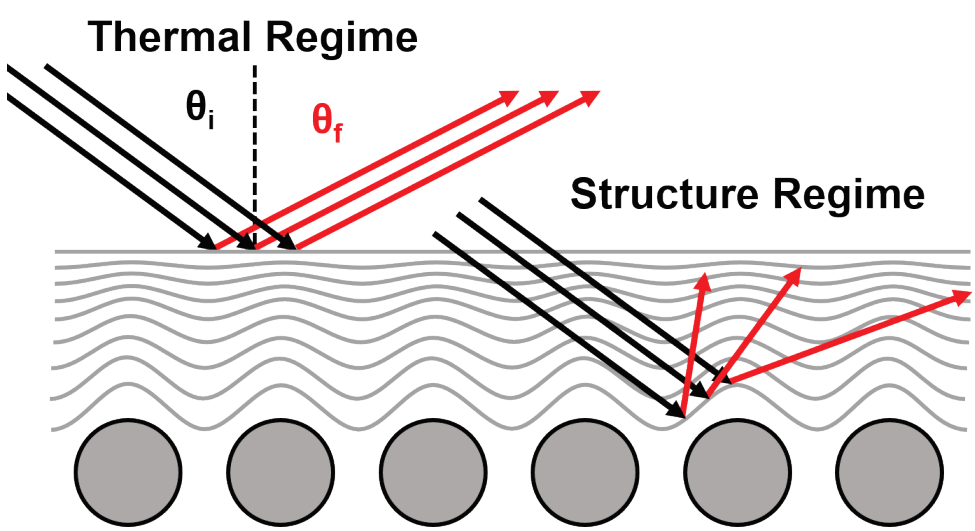

Figure 2.4. Schematic representation of scattering in the thermal and structural scattering regime. The gray circles represent the ion cores of the surface atoms. The grey lines represent the surface potential as a function of distance from the ion cores.

left side). The parallel momentum of the molecule is conserved during the collision because there are no in-plane forces acting on the incoming molecule during the collision. The angular dependence of E_f follows the trend (Figure 2.5, black line)

$$\frac{E_f}{E_i} = \frac{\sin^2(\theta_i)}{\sin^2(\theta_f)}. \tag{2.3}$$

As E_i is increased, the molecule can penetrate deeper into the potential and sample the corrugation of the individual ion cores of the surface (Figure 2.4, right side). The parallel momentum of the molecule is no longer conserved during the collision, and the E_f will increase with θ_f (Figure 2.5, blue symbols). Several models have been developed to model the energy transfer for scattering in the structural regime,[8] including a soft sphere model.[9]

The angular distributions for IS molecules are lobular, with a maximum flux at θ_f away from the surface normal (Figure 2.6). The IS angular distributions are asymmetric about the surface normal ($\theta_f = 0°$). As E_i is increased, the width of the angular distributions will grow broader as the molecule samples more of the surface corrugation. Additionally, the angular distributions will grow broader as the surface roughness of the sample increases. The angular distributions shift past the specular angle ($\theta_i = \theta_f$) as the molecule loses more normal energy, E_n, to the surface, where $E_n = E_i \cos(\theta_i)$. As the surface temperature increases, the angular distributions grow broader as the thermal vibrations of the surface cause more of the molecules to scatter toward the surface normal.[10]

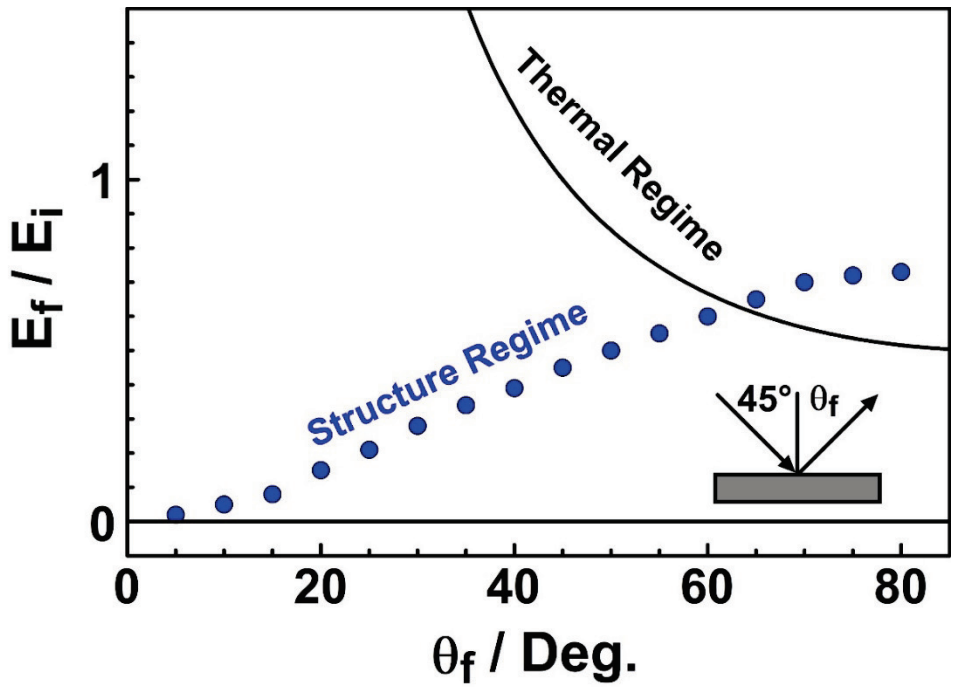

Figure 2.5. The final energy of the scattered molecules, E_f, normalized by the incidence energy, E_i, for molecules with θ_i = 45°. The black line represents E_f / E_i typical of scattering in the thermal regime (from eq 2.3). The blue symbols represent E_f / E_i characteristic of scattering in the structural regime.

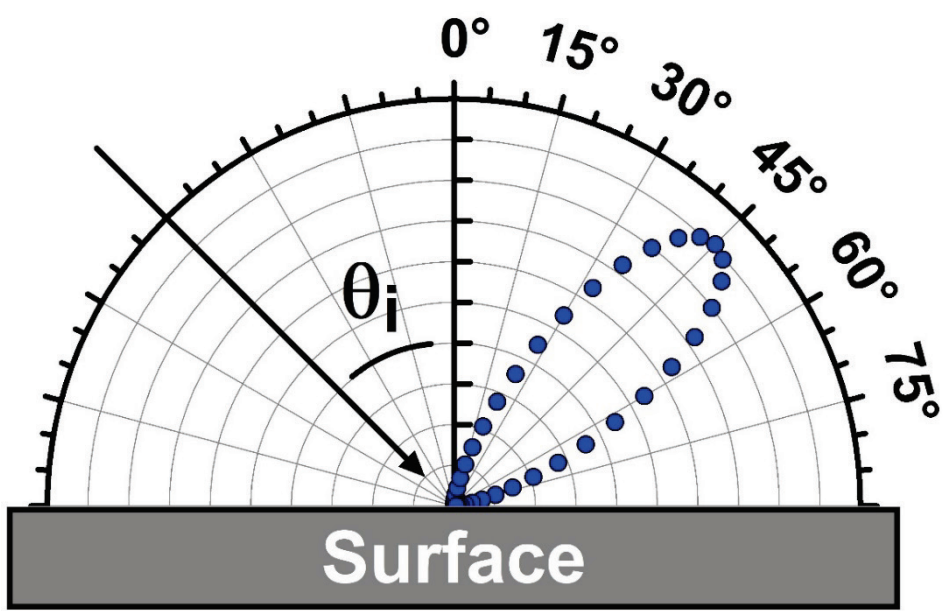

Figure 2.6. An example angular distribution for molecules scattering via the IS channel.

2.1B Thermal Desorption and Detailed Balance

If the incident molecule transfers a substantial amount of energy during the collision, it can "stick" or "trap" in the well of the potential energy surface (Figure 2.3, red curve). If the surface temperature is high enough, the particle can desorb into the vacuum.[11] This scattering mechanism is referred to as thermal desorption (TD). The TD molecules have low translational energies and appear as a broad feature in the TOF distributions (Figure 2.1, red curve). If there is no dependence of the sticking probability on E_i or θ_i, the $P(E_T)$ distribution can be described by a Maxwell Boltzmann distribution of energies (eq 2.4) characterized by the surface temperature, T_s, and the angular distribution of the scattered flux can be described by a $\cos(\theta_f)$ distribution that is symmetric about the surface normal (Figure 2.7, blue curve).

$$P(E_T)_{TD} = E_T \exp\left(-\frac{E_T}{RT_s}\right) \tag{2.4}$$

These observations, referred to as Knudsen's Cosine Law, can be explained using the principle of detailed balance which states that at equilibrium, the flux of particles with velocity v_i incident on the surface is matched by an equal, but opposite, flux leaving the surface with $v_f = v_i$. The flux of molecules on the surface is proportional to the perpendicular *velocity* of the incoming particle:

$$I_i \propto v_i \cos(\theta_i) \tag{2.5}$$

By the principle of detailed balance, the flux of the desorbing particles, which is equal but opposite to the incoming particles, must also be proportional to $\cos(\theta_f)$ and $v_f = v_i$.

Knudsen's Cosine Law applies when the sticking probability of the molecules on the surface, $D(E_T, \theta_i)$, does not depend on E_i or θ_i. However, in some systems, $D(E_T, \theta_i)$

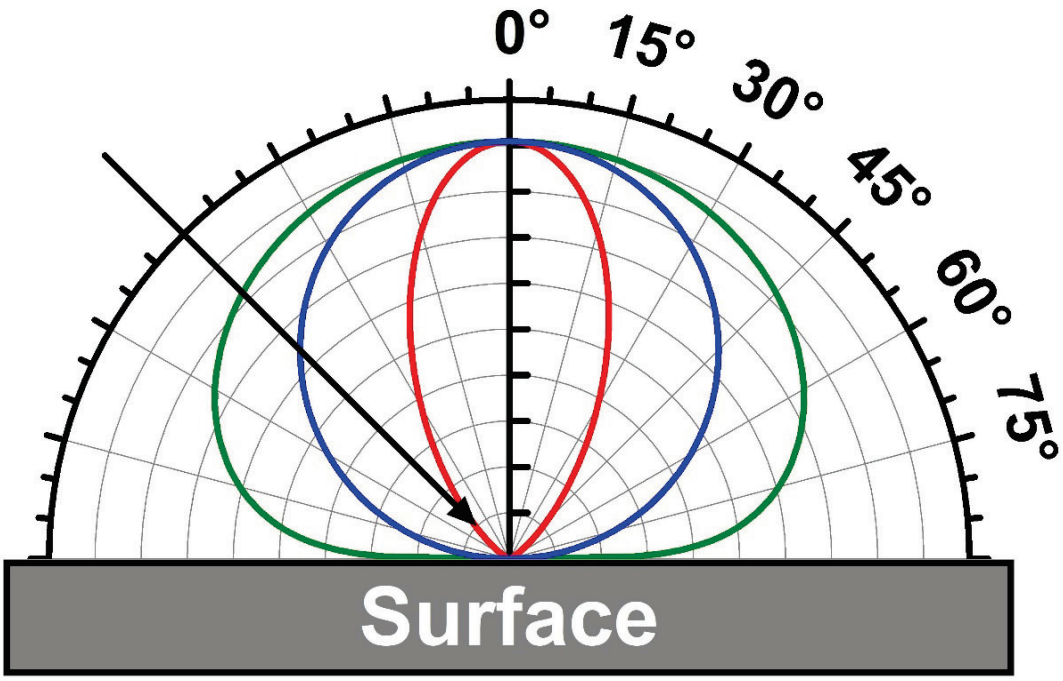

Figure 2.7. Representative angular distributions for molecules exiting the surface via the thermal desorption channel. The blue line represents the angular distribution when the sticking probability does not depend on E_i or θ_i. The green line represents an angular distribution when the sticking probability follows the trend described by $\beta(E_T, \theta_i)$. The red line represents an angular distribution when the sticking probability follows the trend described by $S(E_T, \theta_i)$.

depends on the incident conditions of the incoming particles. Thus, the flux of particles that adsorb to (or desorb from) the surface is a product of the incident (or desorbing) flux, which is described by a Maxwell-Boltzmann distribution of energies in eq 2.4 (Figure 2.8, dashed green curve), and the energy- and angle- dependent sticking probability, $D(E_T, \theta_i)$[12, 13]

$$P(E_T, \theta_f)dE_T d\theta_f = E_T \exp\left(-\frac{E_T}{RT_s}\right) D(E_T, \theta_i)dE_T d\theta_i \qquad (2.6)$$

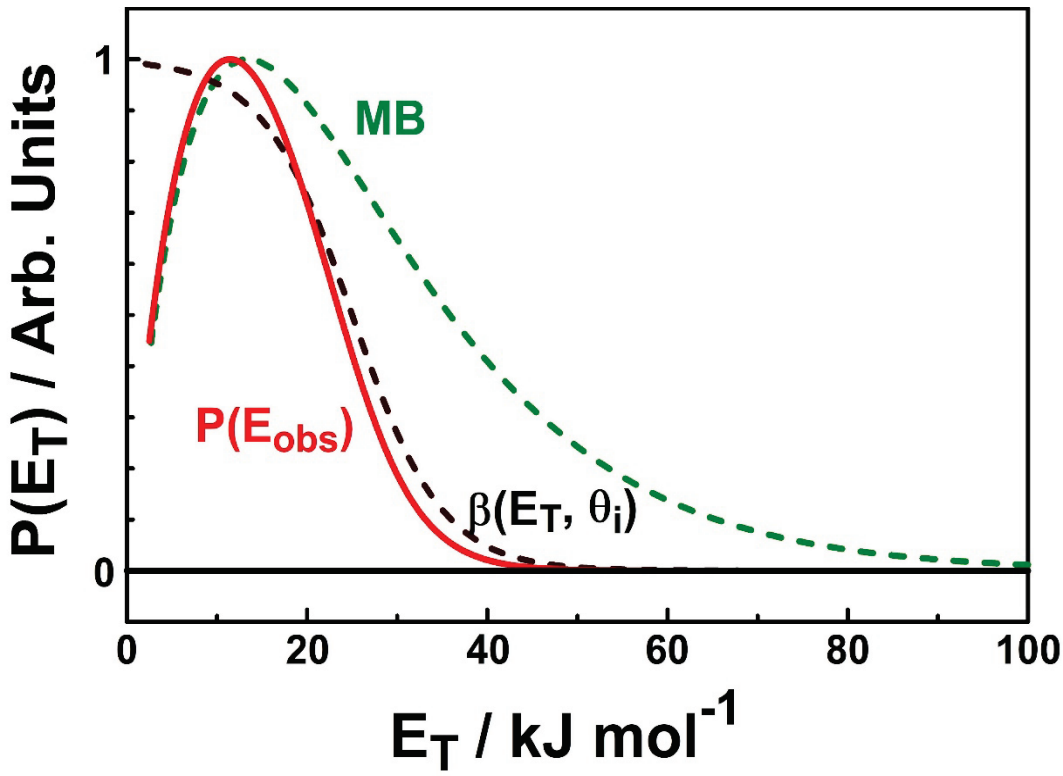

Figure 2.8. Translational energy distribution for products desorbing from the surface after adsorbing via a nonactivated process (red line). The red line is the product of a MB distribution characterized by the surface temperature (dashed green line) and the energy dependent sticking probability for a nonactivated adsorption process, $\beta(E_T, \theta_i)$ (dashed black line).

where E_T is the translational energy (eq 2.2). $D(E_T, \theta_i)$ is determined by varying the E_i or θ_i and measuring the fraction of molecules that stick to the surface. This curve can be used to predict the $P(E_T)$ distribution for the desorbing molecules using eq 2.6 as is shown in Figure 2.8 and 2.12. The functional form of $D(E_T, \theta_i)$ depends on whether the adsorption process is nonactivated or activated.

2.1C Nonactivated Adsorption/Desorption

If the adsorption process is nonactivated (represented in Figure 2.3, red curve), the number of molecules that adsorb to the surface will decrease as E_i exceeds the magnitude of the well depth of the potential energy surface. Thus, lower energy particles will stick preferentially on the surface.

Accordingly, the desorbing particles will appear to have a $P(E_T)$ distribution that is shifted to lower E_T than predicted by a MB distribution characterized by the surface temperature (Figure 2.8, red curve). For an idealized surface, the sticking probability for nonactivated adsorption, $\beta(E_T, \theta_f)$, will be unity until E_i is raised above a critical energy, E_c, where it will fall to zero. This step function is smoothed out by thermal vibrations of the surface and can be expressed by the functional form[12] (Figure 2.8, dashed black curve)

$$D(E_T, \theta_i) = \beta(E_T, \theta_i) = A\left[1 + \exp\left(\frac{E_{eff} - E_c}{X}\right)\right]^{-1} \tag{2.7}$$

where A is a normalization constant (unitless), E_c is the critical energy above which the sticking probability falls to zero (kJ mol^{-1}), and X determines the width of the curve (kJ mol^{-1}). Eq 2.7 depends on the E_i and θ_i by the term E_{eff}:

$$E_{eff} = E_i \cos^n \theta_i \tag{2.8}$$

where n can have values from 0 to 2. When $n = 0$, the sticking probability does not depend on E_i or θ_i, and particles with any energy and orientation will trap with equal probability. For desorbing particles, this means that the E_f will be constant with θ_f and the angular distribution that can be described by a $\cos(\theta_f)$ distribution, as discussed above. When $n = 2$, only energy oriented normal to the surface, E_n, must be dissipated for the particle to trap. The sticking probability increases with θ_i because the particles need to dissipate less energy as θ_i becomes more grazing (Figure 2.9). Accordingly, the desorption of particles that initially adsorbed in a nonactivated process will lead to an angular distribution that is broader than cosine (Figure 2.7, green curve). Simply put, because more molecules adsorb at large θ_i, the flux of desorbing particles will increase with θ_f.

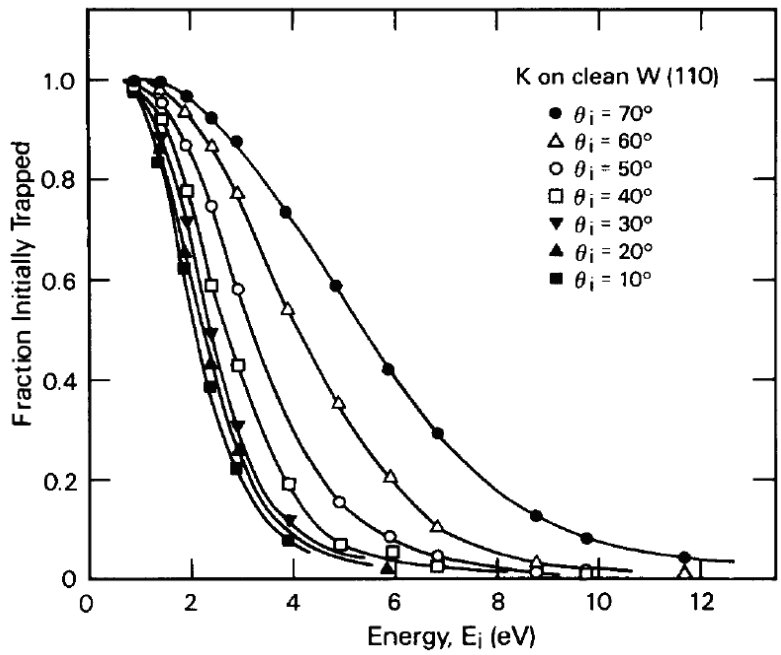

Figure 2.9. The $\beta(E_T, \theta_i)$ for K sticking on a W(110) surface held at a temperature of 1150 K. (Figure from Ref [44]. Data displayed is from Ref. [189] and [190].)

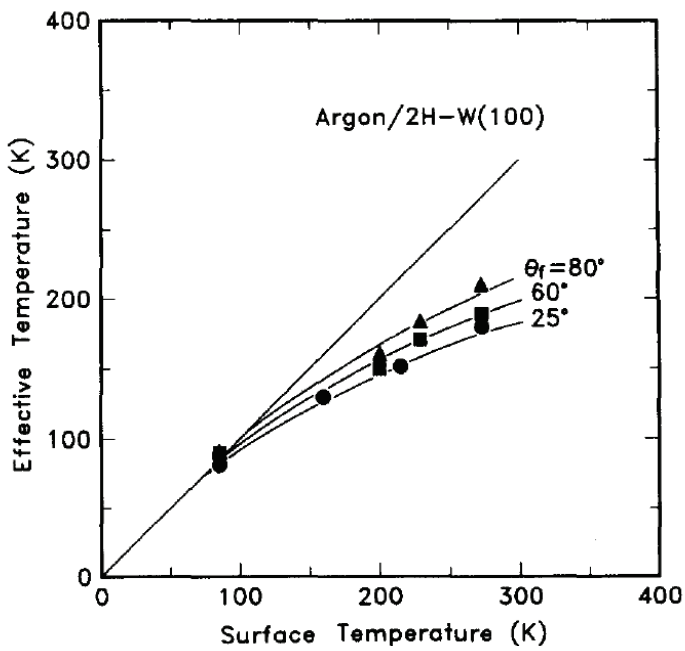

Figure 2.10. The effective temperature of Ar scattering from a hydrogen covered tungsten surface for $\theta_f = 25°$, 60°, and 80°. The E_f of the scattered atoms is proportional to T_{eff}. The energy of the surface, E_s, is equal to $2RT_s$. The black line indicates E_f when it is fully accommodated to E_s. The E_f for $\theta_f = 80°$ is greater than E_f for $\theta_f = 25°$. Figure is from Ref. [39].

Additionally, because the energy oriented parallel to the surface is retained during the collision and only E_n is accommodated, E_f will increase with θ_f (Figure 2.10).

2.1D Activated Adsorption/Desorption

For an activated adsorption process, also referred to as chemisorption, the molecules must surmount a barrier in order enter the potential well (Figure 2.11, red curve). For an ideal surface, the sticking probability, $S(E_T, \theta_i)$, will be a step function that has a value of zero until E_i exceeds the magnitude of the barrier, E_0. For a real surface, thermal vibrations and defects will smooth out the step function and $S(E_T, \theta_i)$ can be expressed by the functional form[14] (Figure 2.12, dashed black line)

$$D(E_T, \theta_f) = S(E_T, \theta_f) = \frac{A}{2}\left[1 + \tanh\left(\frac{E_{eff} - E_0}{W}\right)\right] \qquad (2.9)$$

where E_0 represents the barrier for desorption (kJ mol^{-1}), W is related to the range of desorption barriers arising from the variety of surface sites available for desorption (kJ mol^{-1}), A is a normalization factor (unitless), and E_{eff} is given by eq 2.4. Molecules with high E_i adsorb preferentially to the surface. Accordingly, the desorbing particles will appear to have a $P(E_T)$ distribution that is shifted to higher translational energies than predicted by a MB distribution (Figure 2.12, green line). For adsorption over a barrier, only products with sufficient E_n surmount the barrier and the flux of adsorbed particles will increase as θ_i approaches the surface normal (θ_i = 0°). It follows that the flux of particles that desorb over the barrier will be focused toward the surface normal (θ_f = 0°) and the angular distribution will be narrower than cosine (Figure 2.7, red curve).

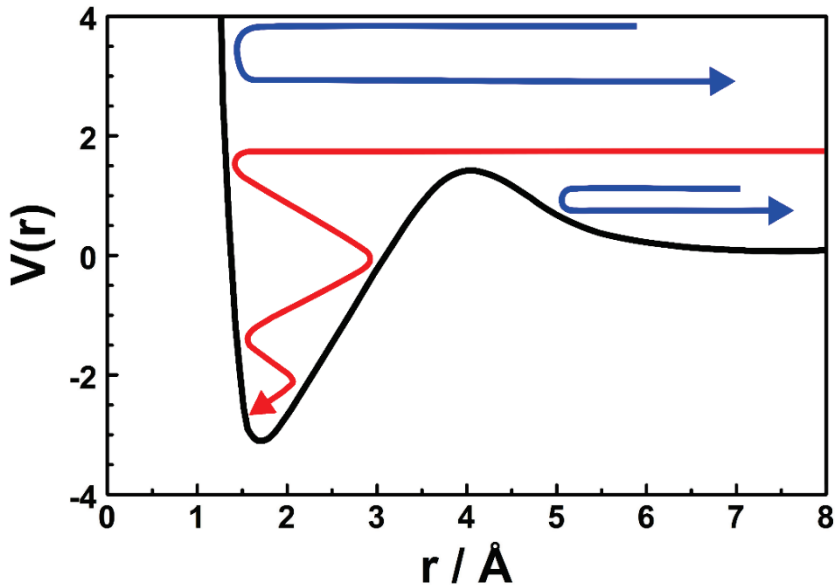

Figure 2.11. Example of a one-dimensional potential energy surface with a barrier to adsorption; r is the distance between the molecule and the surface. The position of the surface is defined as r = 0 Å. The blue line represents molecules that scatter via an IS mechanism from the repulsive wall of the chemisorption well (top blue curve) and from the barrier (dashed blue curve). The red line represents molecules that stick to the surface before exiting the surface via a TD mechanism.

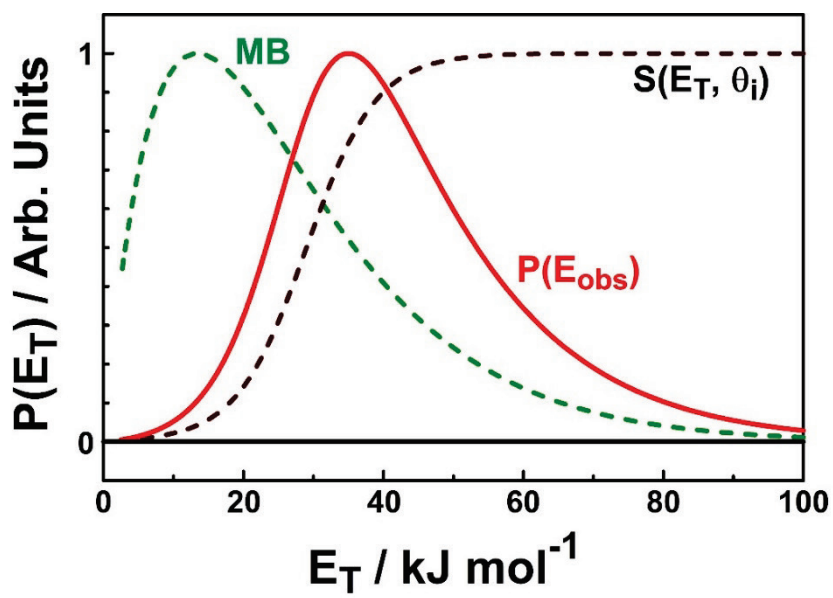

Figure 2.12. Translational energy distribution for products desorbing from the surface after absorbing via an activated process (red line). The red line is the product of a MB distribution characterized by the surface temperature (dashed green line) and the energy dependent sticking probability for a nonactivated adsorption process, $S(E_T, \theta_i)$ (dashed black line).

2.1E Thermal Desorption at High Temperature

In order for a molecule to accommodate to the surface, both the momentum oriented normal and parallel to the surface must be fully dissipated. The normal momentum has been shown to accommodate rapidly, often during the first gas-surface interaction. On a smooth surface, the parallel momentum is accommodated on a much longer time scale because there are few no in plane forces acting on the molecule.[15] At low surface temperature, the residence time of the molecule on the surface is sufficiently long to dissipate the parallel momentum. Thus, the molecule loses all memory of its incidence conditions and the desorbing molecules can be described using the procedure in 2.1C, as described in the previous section. At high temperatures, the residence time decreases and the molecules can escape the surface before the parallel momentum is fully accommodated. Thus, the molecule retains some memory of its incidence conditions and scatters with a lobular distribution that is directed away from the surface normal (Figure 2.13a).[15, 16] The E_f will increase with θ_f because the molecule retains its parallel momentum (Figure 2.13b). This mechanism has been referred to as "quasitrapping".

2.1F Thermal Desorption Following a Residence Time on the Surface

The molecule may reside on the surface for some time after coming into thermal equilibrium.[17] The residence time, τ, can decouple the desorption time from the time at which an incident molecule strikes the surface (Figure 2.14, inset). Thus, the scattered particles will appear to have $P(E_T)$ distributions that are shifted to lower translational energies than predicted by a MB distribution (Figure 2.14, red curve). The residence time can be determined from a gas-surface scattering experiment that employs a pulsed

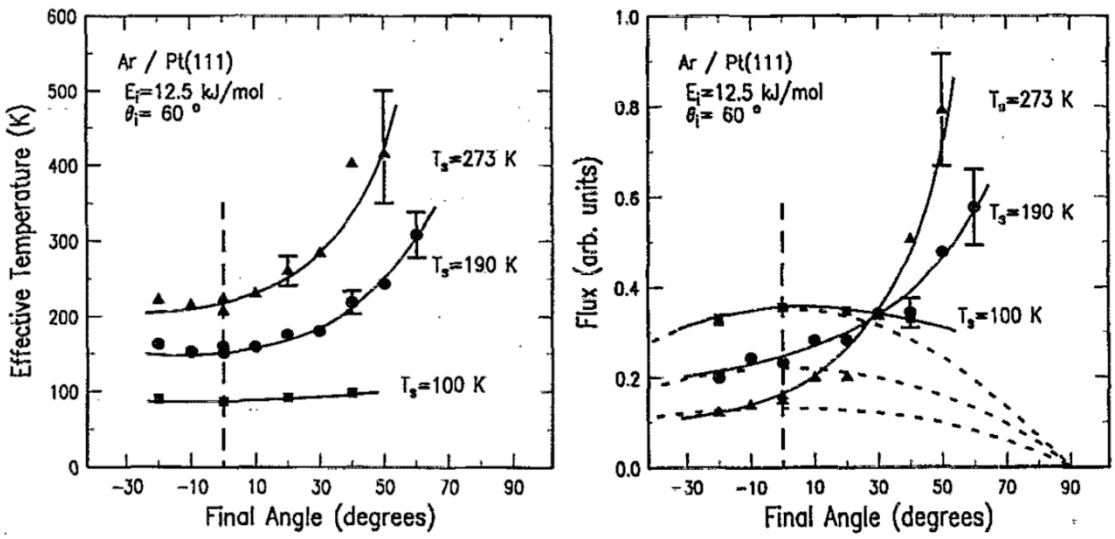

Figure 2.13. The effective temperature (left panel) and flux (right panel) of Ar scattering from a Pt(111) surface held at a temperature of 100, 190, 273 K. The E_f of the scattered atoms is proportional to T_{eff}. Figures are from Ref. [42].

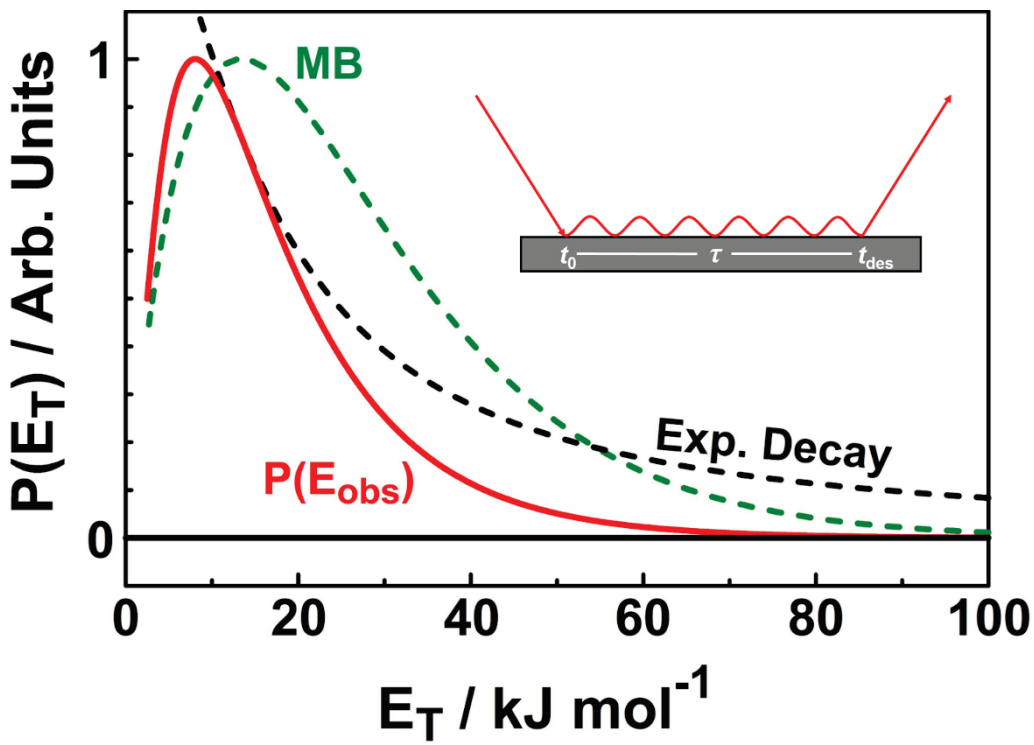

Figure 2.14. Translational energy distribution for products with residence time, τ, desorbing from the surface (red line). The red line is the product of a MB distribution characterized by the surface temperature (dashed green line) and a first order, exponential decay (dashed black line).

molecular beam, as is described in Chapters 3, 4, and 5. The residence time can be determined by fitting the scattered $P(E_T)$ distribution with the convolution of a first order exponential decay (Figure 2.14, dashed black curve) and a MB distribution (Figure 2.14, dashed green curve). To determine the true scattered flux and E_f of the scattered products, which depend directly on the flight time (t), the TOF distributions must be corrected for the residence time of the molecule on the surface.

2.2 Reactive Scattering

The reactive analogues of IS and TD mechanisms are Eley-Rideal (ER) and Langmuir-Hinshelwood (LH) reactions, respectively. A third reactive process, referred to as a "hot-atom" (HA) reaction, is also possible. These reactions can often be distinguished using beam-surface scattering techniques.

2.2A Eley-Rideal Reactions

In an ER reaction, a gas-phase atom abstracts an atom adsorbed on the surface.[18] ER reactions are probable when the surface coverage of the adsorbate is high and the adsorbate is weakly bound to the surface.[19, 20] The incident atom and product molecule do not come into thermal equilibrium with the surface; therefore, the product flux does not depend on surface temperature.[21] Products that are formed by an ER mechanism have memory of the incident reactant's trajectory and have lobular angular distributions (see example in 2.6). The molecules are highly translationally excited,[19, 22] and appear at short flight times in the TOF distributions (Figure 2.1, blue curve). Additionally, a large fraction of the E_i and reaction energy is deposited into internal modes of the molecule. Thus, molecules that are produced by an ER mechanism are highly vibrationally excited.[19, 22]

2.2B Hot Atom Reactions

During an HA reaction, the incident atom enters a quasi-bound state and skips along the surface before reacting with an adsorbate.[23] This reaction does not occur in thermal equilibrium with the surface and the rate is independent of the surface temperature.[21] Products formed by an HA mechanism also have a lobular angular distribution and are translationally and internally excited.[19, 22] Consequently, products of ER and HA reactions are difficult to distinguish without aid from simulations. However, HA reactions are favored over ER reactions when the surface coverage is low and when the adsorbate is tightly bound to the surface.[19, 20]

2.2C Langmuir-Hinshelwood Reactions

An incident atom must first come into thermal equilibrium with the surface before it can react with an adsorbate via a LH reaction mechanism.[18] The reaction occurs in thermal equilibrium with the surface and the product flux depends directly on the temperature of the surface. The energy released during the reaction is deposited into the surface and the product molecules have a translational and internal energy distribution that are in equilibrium with the surface. Accordingly, the products desorb into the vacuum with low translational energies and appear at large flight times in the TOF distributions (Figure 2.1 red curve). If there is no barrier to desorption, the product molecule desorbs with a cosine angular distribution and E_f that follow Knudsen's Cosine Law (Figure 2.7, blue curve). If there is a barrier to desorption, the product molecule has an angular distribution that is narrower than cosine and energies that are greater than expected by a MB distribution as described in section 2.1D.[13] If there is a residence time associated with the reaction, the product molecules will appear to be exiting the surface with energies lower than predicted by a MB distribution and the analysis described in Section 2.1F must be followed.[17]

References

1. Olander, D. R.; Schwarz, J. A.; Siekhaus, W.; Jones, R. Reactions of Modulated Molecular-Beams with Pyrolytic-Graphite: 1. Oxidation of Basal Plane. *J. Chem. Phys.* **1972**, *57*, 408-420.

2. Rosner, D. E.; Allendor.Hd Comparative Studies of Attack of Pyrolytic and Isotropic Graphite by Atomic and Molecular Oxygen. *AIAA J.* **1968**, *6*, 650-654.

3. Rosner, D. E.; Allendorf, H. D. High Temperature Oxidation of Carbon by Atomic Oxygen. *Carbon* **1965**, *3*, 153-156.

4. Bonn, M.; Kleyn, A. W.; Kroes, G. J. Real Time Chemical Dynamics at Surfaces. *Surf. Sci.* **2002**, *500*, 475-499.

5. Zhang, J.; Garton, D. J.; Minton, T. K. Reactive and Inelastic Scattering Dynamics of Hyperthermal Oxygen Atoms on a Saturated Hydrocarbon Surface. *J. Chem. Phys.* **2002**, *117*, 6239-6251.

6. Minton, T. K.; Giapis, K. P.; Moore, T. Inelastic Scattering Dynamics of Hyperthermal Fluorine Atoms on a Fluorinated Silicon Surface. *J. Phys. Chem. A* **1997**, *101*, 6549-6555.

7. Rettner, C. T.; Barker, J. A.; Bethune, D. S. Angular and Velocity Distributions Characteristic of the Transition Between the Thermal and Structure Regimes of Gas-Surface Scattering. *Phys. Rev. Lett.* **1991**, *67*, 2183-2186.

8. Lahaye, R. J. W. E.; Kang, H. Energy Exchange in Structure scattering: a Molecular Dynamics Study for Cs+ from Pt(111). *Surf. Sci.* **2001**, *490*, 327-335.

9. Alexander, W. A.; Zhang, J.; Murray, V. J.; Nathanson, G. M.; Minton, T. K. Kinematics and Dynamics of Atomic-Beam Scattering on Liquid and Self-Assembled Monolayer Surfaces. *Faraday Discuss.* **2012**, *157*, 355-374.

10. Hurst, J. E.; Wharton, L.; Janda, K. C.; Auerbach, D. J. Direct Inelastic Scattering Ar from Pt(111). *J. Chem. Phys.* **1983**, *78*, 1559-1581.

11. Hurst, J. E.; Becker, C. A.; Cowin, J. P.; Janda, K. C.; Wharton, L.; Auerbach, D. J. Observation of Direct Inelastic Scattering in the Presence of Trapping-Desorption Scattering: Xe on Pt(111). *Phys. Rev. Lett.* **1979**, *43*, 1175-1177.

12. Rettner, C. T.; Schweizer, E. K.; Mullins, C. B. Desorption and Trapping of Argon at a 2H-W(100) Surface and a Test of the Applicability of Detailed Balance to a Nonequilibrium System. *J. Chem. Phys.* **1989**, *90*, 3800-3813.

13. Michelsen, H. A.; Auerbach, D. J. A Critical Examination of Data on the Dissociative Adsorption and Associative Desorption of Hydrogen at Copper Surfaces. *J. Chem. Phys.* **1991**, *94*, 7502-7520.

14. Harris, J. On Vibrationally-Assisted Dissociation of H_2 at Metal Surfaces. *Surf. Sci.* **1989**, *221*, 335-345.

15. Head-Gordon, M.; Tully, J. C.; Rettner, C. T.; Mullins, C. B.; Auerbach, D. J. On the Nature of Trapping and Desorption at High Surface Temperatures. Theory and Experiments for the Ar–Pt(111) System. *J. Chem. Phys.* **1991**, *94*, 1516-1527.

16. Majumder, M.; Bhandari, H. N.; Pratihar, S.; Hase, W. L. Chemical Dynamics Simulation of Low Energy N_2 Collisions with Graphite. *J. Phys. Chem. C* **2018**, *122*, 612-623.

17. Barker, J. A.; Auerbach, D. J. Gas-Surface Interactions and Dynamics; Thermal energy Atomic and Molecular Beam Studies. *Surf. Sci. Rep.* **1984**, *4*, 1-99.

18. Kleyn, A. W. Molecular Beams and Chemical Dynamics at Surfaces. *Chem. Soc. Rev.* **2003**, *32*, 87-95.

19. Pétuya, R.; Larrégaray, P.; Crespos, C.; Aurel, P.; Busnengo, H. F.; Martínez, A. E. Scattering of Atomic Hydrogen Off a H-Covered W(110) Surface: Hot-Atom versus Eley–Rideal Abstraction Dynamics. *J. Chem. Phys. C* **2015**, *119*, 3171-3179.

20. Zecho, T.; Güttler, A.; Sha, X.; Lemoine, D.; Jackson, B.; Küppers, J. Abstraction of D Chemisorbed on Graphite (0001) with Gaseous H Atoms. *Chem. Phys. Lett.* **2002**, *366*, 188-195.

21. Quintas-Sánchez, E.; Larrégaray, P.; Crespos, C.; Martin-Gondre, L.; Rubayo-Soneira, J.; Rayez, J.-C. Dynamical Reaction Pathways in Eley-Rideal Recombination of Nitrogen from W(100). *J. Chem. Phys.* **2012**, *137*, 064709.

22. Zaharia, T.; Kleyn, A. W.; Gleeson, M. A. Eley-Rideal Reactions with N Atoms at Ru(0001): Formation of NO and N_2. *Phys. Rev. Lett.* **2014**, *113*, 053201.

23. Harris, J.; Kasemo, B. On Precursor Mechanisms for Surface Reactions. *Surf. Sci.* **1981**, *105*, L281-L287.